Quality factor based design guideline for optimized inductive power transfer

Grazian, Francesca; Shi, Wenli; Soeiro, Thiago B.; Dong, Jianning; van Duijsen, Peter; Bauer, Pavol

Quality Factor Based Design Guideline for Optimized Inductive Power Transfer

Francesca Grazian, Wenli Shi, Thiago B. Soeiro, Jianning Dong, Peter van Duijsen and Pavol Bauer

DC System Energy conversion and Storage (DCE&S)
Delft University of Technology
Delft, The Netherlands
Email: (F.Grazian, W.Shi-3, T.BatistaSoeiro, J.Dong-4, P.J.vanDuijsen, P.Bauer)@tudelft.nl

Abstract—In high-power wireless battery charging that uses inductive power transfer, a considerable amount of power losses are located in the transmitter and receiver coils because they carry high resonant currents and typically have a loose coupling between them which increases eddy current losses. Therefore, the nominal operation needs to be chosen such that the coils' losses are minimized. Additionally, the inverter's semiconductors soft-switching improves both the power conversion efficiency and the electromagnetic compatibility of the system, thus it needs to be safeguarded for a wide operating range. However, depending on the chosen quality factor of the coils, it might happen that the minimum coils' losses and soft-switching are not satisfied at the same time. This paper defines a guideline on the parametric selection of the coils' quality factor such that the optimum operation of both the coils and the resonant converter can be achieved simultaneously. This parametric guideline is proposed for resonant converters implementing the four basic compensation networks: series-series, series-parallel, parallel-series, and parallel-parallel. Finally, circuit examples are provided for an 11 kW wireless battery charging system.

Index Terms—Compensation networks, EV battery charging, inductive power transfer, quality factor, wireless charging.

I. INTRODUCTION

Wireless Power Transfer (WPT) for battery charging of electric vehicles (EVs) is pointing towards high power levels such that the duration of the charging process can be shortened. Especially in these high-power applications, the inductive power transfer (IPT) with magnetic resonant coupling is the most used method. Available standards and regulations cover power levels from $3.3\,\mathrm{kW}$ up to $22\,\mathrm{kW}$ [1], which should be processed at the nominal operating frequency of around $85\,\mathrm{kHz}$. As a result, in the IPT system, the resonant current flowing through both the transmitter and receiver coils might have a relatively high amplitude. Finally, due to the standardized coil dimensions and operating range limits, the losses in the system can be considerably high, and thus, it is important to minimize them during the operation to achieve acceptable power efficiency.

From the power electronics point of view, it is fundamental to maintain the soft-switching of the inverter at the transmitter side to increase the efficiency and, above all, to limit the semiconductor stress in order to safeguard the switches reliability. The latter is particularly true for high voltage Si-based MOSFETs which suffer poor body-diode reverse recovery performance that can reduce the switch lifetime during hard-

switching operation. According to [2], the soft-switching can be achieved by operating the typical H-bridge inverter shown in Fig. 1(a) at a frequency higher than the compensation network's natural resonant frequency. In this way, the current flowing from the inverter lags the fundamental H-bridge's generated voltage, displaying a inductive-like behavior which should be able to completely discharge the output capacitance of the switches and other parasitic capacitance at the turn-on. By guaranteeing operation above the resonance frequency during the time interval immediately after a MOSFET has turned off, i.e. during the dead time, a smooth transition occurs thanks to the charging and discharging of the lump equivalent parasitic capacitances within the commutation loop. After the bridge-leg capacitance charges are completely exchanged, the body-diode of the other MOSFET to be turned-on starts conducting the impressed current. Finally, the MOSFET can be turned on ensuring a zero-voltage switching (ZVS). To achieve an inductive behavior at an operating frequency higher than the resonant, the phase angle of the inverter's output current in relation to the generated voltage must be monotonic with respect to the frequency. However, depending on both the loading condition and magnetic interaction between the primary and secondary coils, the phase angle of the transmitter current might have multiple zero crossings, which means that it is not monotonic. In the literature, this condition is called bifurcation phenomenon or frequency splitting [3]–[8]. In those cases, operating above the resonant frequency leads to a capacitive-like behavior of the transmitter current that causes hard-switching at the turn-on. Therefore, to guarantee soft-switching, the operation must be bifurcation-free.

All in all, depending on the paramenters' selection of the wireless battery charging system, the condition that minimizes the coils' losses and the one that ensures ZVS turn-on of the inverter might not be satisfied by the same operating condition. Therefore, this paper defines a guideline on the selection of coils' quality factor that ensures the optimum coils' operation and bifurcation-free condition simultaneously. This parametric guideline is proposed for the four basic compensation networks of a resonant converter: series-series (S-S), series-parallel (S-P), parallel-series (P-S), and parallel-parallel (P-P), which mainly differ in the placement of the capacitors that compensate the reactive power of the coils [9]. The definition of this guideline can be found in Section II, together with
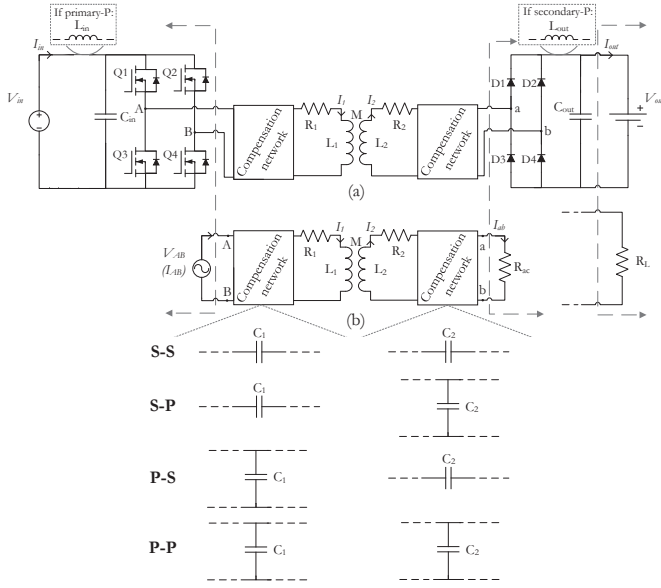
Fig. 1. Equivalent circuit of the four basic compensation networks (S-S, S-P, P-S, P-P): (a) complete system, (b) phasor equivalent circuit.

Secondary Compensation	Q_{1c}	Q_{2c}	$R_{ac,opt}$
S	$\dfrac{\omega_0 L_1}{R_1}$	$\dfrac{\omega_0 L_2}{R_2}$	$\sqrt{\dfrac{L_2}{C_2}}\dfrac{\sqrt{1+k^2 Q_{1c}Q_{2c}}}{Q_{2c}}$
P			$\sqrt{\dfrac{L_2}{C_2}}\dfrac{Q_{2c}}{\sqrt{1+k^2 Q_{1c}Q_{2c}}}$

TABLE II
STABILITY (BIFURCATION-FREE) CRITERIA [9], WHERE THE CIRCUIT QUALITY FACTORS Q_1, Q_2 ARE DEFINED IN TABLE III.

S-S	$Q_1 > \dfrac{4Q_2^3}{4Q_2^2 - 1}$	$R_{ac,bif} > \omega_0 L_2 \sqrt{2(1-\sqrt{1-k^2})}$
S-P	$Q_1 > Q_2 + \dfrac{1}{Q_2}$	$R_{ac,bif} < \sqrt{\dfrac{\omega_0^2 L_1 L_2^3}{M^2} - \omega_0^2 L_2^2}$
P-P		
P-S	$Q_1 > Q_2$	$R_{ac,bif} > \omega_0 M \sqrt{\dfrac{L_2}{L_1}}$

TABLE III
REFLECTED RESISTANCE R_r, REFLECTED REACTANCE X_r, PRIMARY AND SECONDARY CIRCUIT QUALITY FACTORS Q_1, Q_2 [9].

Secondary Compensation	R_r	X_r	Q_1	Q_2
S	$\dfrac{\omega_0^2 M^2}{R_{ac}}$	0	$\dfrac{L_1 R_{ac}}{\omega_0 M^2}$	$\dfrac{\omega_0 L_2}{R_{ac}}$
P	$\dfrac{M^2 R_{ac}}{L_2^2}$	$-\dfrac{\omega_0 M^2}{L_2}$	$\dfrac{\omega_0 L_1 L_2^2}{M^2 R_{ac}}$	$\dfrac{R_{ac}}{\omega_0 L_2}$

the circuit derivation process. According to this guideline, example designs of 11 kW wireless charging systems can be found in Section III for all the compensation networks. Section IV includes extra conditions on the guideline such that it is still valid also in the presence of circuit parameters' variation that might be due to manufacturing tolerance, degradation, or temperature rise. Finally, in Section V, conclusions on the proposed parametric guideline are presented.

II. DEFINITION OF THE PARAMETRIC GUIDELINE

To reach high efficiency of an EV wireless charging system, it is beneficial to minimize the coils' losses. According to [10], it is possible to reach the maximum efficiency of the coils by operating the system at a specific equivalent resistive optimum load $R_{L,opt}$. Considering as a reference the circuit diagram in Fig. 1 that can use the S-S, S-P, P-S, or P-P compensation, the operation needs to satisfy (1). The phasor convention is used to analyze the complete system in Fig. 1(a) which results in the equivalent circuit in Fig. 1(b). In this analysis, the current and voltage waveforms are considered to be sinusoidal at the fundamental frequency. The equivalent resistive load R_{ac} of the circuit in Fig. 1(b) is defined in (2) for secondary-series compensations, and in (3) for the secondary-parallel ones [11].

$$R_L = \frac{V_{out}}{I_{out}} = R_{L,opt} \tag{1}$$

$$R_{ac} = \frac{8}{\pi^2} R_L \tag{2}$$

$$R_{ac} = \frac{\pi^2}{8} R_L \tag{3}$$

Table I shows the optimum load $R_{ac,opt}$ for the four basic compensation networks, in which Q_{1c} and Q_{2c} are the primary and secondary coil's quality factor, respectively. The higher the quality factor is, the closer the coil behaves to an ideal inductor. On top of this design requirement,

the bifurcation phenomenon has to be taken into account [4]. A bifurcation-free operation is desirable to have full controllability of the inverter. In that case, the phase angle of the equivalent impedance seen by the H-bridge inverter is a monotonic function of the frequency that crosses the zero only at the designed resonant frequency f_0. Therefore, operating above the resonant frequency f_0 guarantees an inductive-like behavior of I_1, where the current coming out of the inverter lags the generated voltage, and consequently, it allows ZVS turn-on of the inverter's semiconductors. In Table II, the boundary $R_{ac,bif}$ that ensures a bifurcation-free operation is given for the four basic compensation networks, where the primary and secondary circuit's quality factors Q_1, Q_2 are defined in Table III. Depending on the chosen design, the range of the bifurcation-free condition in Table II might not include the optimum load $R_{ac,opt}$ in Table I. An example of this incompatibility is shown in [12] for a S-S compensation network, where a sub-optimum design needs to be chosen to prevent the bifurcation phenomenon.

In the design process, it is possible to make sure that the condition for the optimum efficiency of the coils and the bifurcation-free operation are compatible at the same time. This can be done by relating the two conditions to each other. The analytical approach to combine both conditions is shown in Table IV for the basic compensation networks. Once the secondary coil inductance L_2 and series resistance R_2, the operating frequency $\omega_0 = 2\pi f_0$, and the coupling factor k are designed, the primary coil's quality factor Q_{1c}^* that
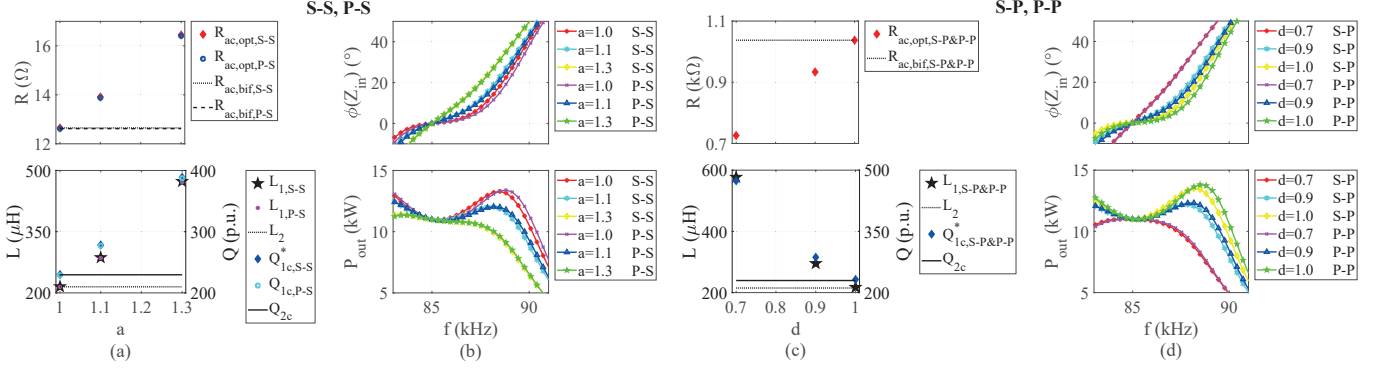
Fig. 2. 11 kW wireless battery charging systems at different values of either the coefficient a for the S-secondary in (a),(b), or d for the P-secondary in (c),(d). (a),(c): optimum load, coils' inductance and quality factor. (b),(d): phase angle of the input impedance and output power depending on the frequency.

TABLE IV
PARAMETRIC CONDITION ON Q_{1c} SUCH THAT BOTH THE OPTIMUM LOAD (TABLE I) AND THE BIFURCATION-FREE CRITERIA (TABLE II) ARE SATISFIED AT THE SAME TIME.

	Design condition	Q_{1c}^*
S-S	$R_{ac,opt} = aR_{ac,bif}$	$\dfrac{2a^2(1-\sqrt{1-k^2})\omega_0^2 L_2^2 - R_2^2}{k^2\omega_0 L_2 R_2}$
S-P	$R_{ac,opt} = dR_{ac,bif}$	$\dfrac{k^2\omega_0 L_2^2 - d^2(1-k^2)R_2^2}{d^2(1-k^2)R_2 k^2\omega_0^2 L_2}$
P-P		
P-S	$R_{ac,opt} = aR_{ac,bif}$	$\dfrac{a^2 k^2\omega_0^2 L_2^2 - R_2}{R_2 k^2\omega_0 L_2}$

where $a > 1$ and $d < 1$

satisfies both conditions can be computed for the four basic compensation networks. In Table IV, the condition on Q_{1c}^* is not strict because it can be tuned by choosing the value of the coefficients a or d. The further a and d are from the unity, the more $R_{ac,opt}$ is going to differ from $R_{ac,bif}$. Wireless charging systems with different a or d coefficients are designed in Section III. Therein, these designs are analyzed in detail to fully understand the differences in their characteristics.

III. IPT SYSTEM DESIGNS AND ANALYSIS

To evaluate the parametric guideline in Table IV, examples of circuit parameters for 11 kW wireless battery charging systems have been computed for the four basic compensation networks at different values of the coefficients a and d. The results are summarized in Fig. 2. To perform such analysis:

- The coefficients a and d assume the values $a = (1, 1.1, 1.3)$, and $d = (0.7, 0.9, 1)$. This means that, for each compensation network, three designs are analyzed which have an optimum load $R_{L,opt}$ that can be equal, 10%, or 30% different from the bifurcation boundary load $R_{L,bif}$;
- The secondary coil in [13] is used as a reference, whose parameters are $L_2 = 214.96\,\mu H$ and $R_2 = 0.5\,\Omega$;
- The primary coil is designed such that $Q_{1c}=Q_{1c}^*$, $k = 0.11$, and $R_1=R_2 \cdot a$ (or $R_1=R_2\cdot(2-d)$). It is assumed that an higher inductance corresponds to a higher series resistance because of an increase in the number of turns;
- The coupling factor k between the coils is fixed.

Fig. 2(a),(c) show the resulting $R_{ac,opt}$ and $R_{ac,bif}$ at the different coefficients a and d. As expected from the design condition in Table IV, $R_{ac,opt}$ and $R_{ac,bif}$ are identical when a and d are equal to the unity. On the other hand, the further a and d are from the unity, the more $R_{ac,opt}$ differs from $R_{ac,bif}$. Additionally, given the above-mentioned assumptions, Fig. 2(a),(c) show also the resulting coils' inductance L_1, L_2, and the coils' quality factors $Q_{1c}=Q_{1c}^*$, Q_{2c}. When $R_{ac,opt} = R_{ac,bif}$, the inductance and quality factor of both coils are equivalent, which means that the primary and secondary coils are identical. The farthest a and d are from the unity, the larger the inductance of the primary coil is with respect to the secondary coil. However, the inductance is not the only parameter changing, because also the coils' quality factor increases as a and d becomes more different than the unity. This means that L_1 is not only increased by adding more turns but also by modifying the coils' geometry and dimensions.

As explained in Section II, the soft-switching of the inverter can be achieved by operating at a frequency higher than the system's resonant one, as long as the condition $a > 1$ or $d < 1$ is valid. However, within this condition, the value of a and d highly influences the phase angle of the input impedance $\phi(Z_{in})$ seen by the inverter in the frequency domain. As a consequence, this affects the controllability of the inverter. Fig. 2(b),(d) show that the farther a and d are from the unity, the steeper $\phi(Z_{in})$ becomes. This means that, with small variations of frequency, considerably higher inductive behavior (phase shift) can be achieved. However, it is not preferable to have a sharp change in $\phi(Z_{in})$ while changing the frequency, because it is important to have a smooth controllability of the reactive power circulating in the system. On the other hand, if the gradient of $\phi(Z_{in})$ is relatively low, it might happen that the desired phase shift cannot be achieved within the allowed frequency range. For example, according to [14], the allowed operating frequency range is 79-90 kHz. Therefore, if the nominal frequency is chosen as 85 kHz, there is a tuning range for the soft-switching of 5 kHz.

Besides the ZVS turn-on, another direct consequence of operating at a frequency slightly higher than the resonance is that the delivered output power P_{out} would vary from the design value. Fig. 2(b),(d) show the characteristic of P_{out}
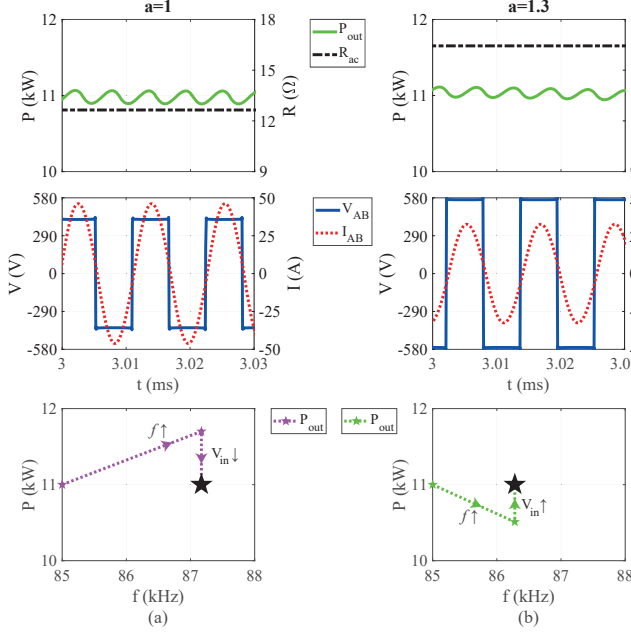
Fig. 3. Operating circuit waveforms of the 11 kW S-S compensation network in Fig. 2 with ZVS turn-on ($f > f_0$), where: (a) a=1, (b) a=1.3.

Fig. 4. DC output V_{out}, I_{out} and DC input source (either V_{in} or I_{in}) at different values of either a or d for: (a) S-S, (b) P-S, (c) S-P, and (d) P-P.

depending on the operating frequency for different values of the coefficient a or d, where it is chosen that $P_{out} = 11$ kW at the resonant frequency of f_0=85 kHz. When a and d are close to the unity, P_{out} increases when operating at frequencies immediately higher than the resonance. This means that the DC input source (either V_{in} or I_{in}) must be lowered to set the value of P_{out} back to the nominal level. This could be done by connecting a step-down converter at the input of the H-bridge inverter. However, above a certain frequency, P_{out} starts dropping and the characteristic required from the DC input source would be the opposite. Therefore, in the case that a and d are close to the unity, the converter connected at the input of the system might need both a step-up and step-down behavior. On the other hand, as the coefficients a and d become farther than the unity, P_{out} drops for the whole frequency range higher than the resonance. As a consequence, the DC input source needs only to be stepped up to reach the nominal P_{out}. In this case, the operation would be inherently safer because of the power would not be higher than the nominal, the controllability of the system becomes easier since it is only required in one direction, and the DC input source range of the converter can be extended since only a step-up converter could be used rather than a step-up and step-down converter. However, as a and d become far from the unity, the effective bandwidth in which it is possible to deliver P_{out} reduces as it is shown in Fig. 2(b),(d). A narrow bandwidth would become critical for the stability of the IPT, which is especially true in the presence of frequency detuning due to the parameters' tolerance. Therefore, it is not preferable to select a value for a and d excessively different than unity. From this example, it is clear that the choice of the coefficients a and d affects also the topology selection for the power electronics converter needed to ensure a stable delivery of P_{out}.
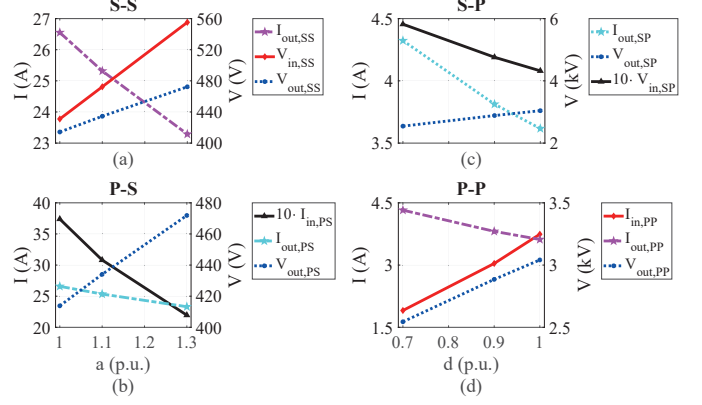
The described characteristics of the resonant converters for IPTs have been also verified through circuit simulations. Fig. 3 shows the circuit waveforms of the 11 kW S-S compensation network designed with a=1 and a=1.3. Thereby, the H-bridge inverter operates at ZVS turn-on with a positive switch current of 8 A, and the equivalent load R_{ac} is set at the computed optimum load $R_{ac,opt}$ in Fig. 2(a). When the operating frequency is increased to achieve the ZVS turn-on, it is possible to observe that P_{out} characteristic agrees with the one in Fig. 2(b): P_{out} increases for a=1 and decreases for a=1.3. As a consequence, the input voltage V_{in} must be controlled to shift P_{out} back to 11 kW. In particular, in Fig. 3(a), V_{in} has been lowered from 431 V to 417 V, while in Fig. 3(c), it has been increased from 555.2 V to 567.2 V.

Additionally, at the resonant frequency, different values of a and d lead to a different voltage and current at both the input and output for the same output power, which highly influence the power transfer characteristic. This influence is shown in Fig. 4 for $P_{out} = 11$ kW. In terms of DC input and output quantities, the value of a and d can be chosen such that V_{in} is within the allowed voltage range from the grid connection, and that V_{out} matches the nominal voltage of the battery.

IV. VALUES OF a AND d BASED ON THE CIRCUIT PARAMETERS' TOLERANCE

Table IV defines a guideline on the value of the primary coil's quality factor Q_{1c} for all the basic compensation networks, such that the optimum operation of the main coils is bifurcation free. According to Fig. 2, it might be preferable to choose a specific value for the coefficient a or d depending on the nature of the DC/DC or AC/DC converter used at the input of the system. However, it is well-known that in reality the circuit parameters might differ from their theoretical value because of the components' manufacturing tolerance, temperature variations, and/or component degradation. In the presence of such parameters' variation, it might occur that the actual resulting a is lower than the unity or that d is greater than the unity, which would lead to the undesirable bifurcation. In this section, the values of the coefficients a and d are computed to ensure the validity of the parametric

TABLE V

TABLE V

VALUES OF THE COEFFICIENTS a AND d, AND THE GAINS $\underline{A}$ AND $\underline{D}$ IN (4) WHEN CONSIDERING THE TOLERANCE OF THE CIRCUIT PARAMETERS.

	Approximation	Coefficient a, or d	$\underline{A}$, or $\underline{D}$
S-S	$k^4(1-k^2) \approx 0$	$k\sqrt{\dfrac{R_2 L_1}{2R_1 L_2}}$	$\underline{k}\sqrt{\dfrac{\underline{r_2}\,\underline{l_1}}{\underline{r_1}\,\underline{l_2}}}$
S-P	$\dfrac{R_1 R_2 C_2}{k^2 L_1} \ll 1$	$\sqrt{\dfrac{R_1 L_2}{R_2 L_1}}\dfrac{1}{\sqrt{1-k^2}}$	$\sqrt{\dfrac{\underline{r_1}\,\underline{l_2}}{\underline{r_2}\,\underline{l_1}}}\sqrt{\dfrac{1-k^2}{1-\underline{k}^2 k^2}}$
P-P			
P-S		$\sqrt{\dfrac{R_2 L_1}{R_1 L_2}}$	$\sqrt{\dfrac{\underline{r_2}\,\underline{l_1}}{\underline{r_1}\,\underline{l_2}}}$

Fig. 5. Worst-case coefficients a' and d' starting from a = (1, 1.1, 1.3), and d = (0.7, 0.9, 1) used in Section III, for: (a) S-S, P-S, and (b) S-P, P-P. The computation uses (4) with the gains $\underline{A}$ and $\underline{D}$ in (5).

guidelines in Table IV when the circuit parameters' tolerance are taken into account.

A parameter tolerance is normally expressed as a percentage of its nominal value. For example, let's assume that the tolerance on L_1 is estimated to be $\pm X \%$. This means that the actual value of the primary inductance L_1' would be $L_1' = \underline{l_1} L_1$ where $\underline{l_1} = (1 \pm \frac{X}{100})$. The same approach can be applied to all the circuit parameters in Fig. 1. By considering all the parameters' tolerance, the actual values of a and d, which are hereby named a' and d', might differ from their theoretical values and, eventually, they might not fulfill anymore the design condition in Table IV. As it is shown in (4), a' and d' can be calculated from a and d by using the gain $\underline{A}$ and $\underline{D}$, respectively. These gains are function of the parameters' tolerance, and they can be computed from Table V.

$$a' = \underline{A}(\underline{k}, \underline{l_1}, \underline{l_2}, \underline{r_1}, \underline{r_2}, \underline{c_1}, \underline{c_2}) \cdot a \quad \text{(S-S \& P-S)}$$
$$d' = \underline{D}(\underline{k}, \underline{l_1}, \underline{l_2}, \underline{r_1}, \underline{r_2}, \underline{c_1}, \underline{c_2}) \cdot d \quad \text{(S-P \& P-P)} \tag{4}$$

The value of a and d can be set by using an iterative process. First, an initial value is assigned to a and d. Then, the value of a' and d' must be calculated while considering the worse case scenario of the parameters' tolerance. If a' and d' still respect the parametric guideline in Table IV, the initially selected value of a and d is suitable and the iteration is ended. Otherwise, another value is assigned to a and d and the iteration starts again from the beginning. For example, let's assume that all the circuit parameters used in the example designs in Section III have a tolerance of $\pm 5 \%$. According to Table V, the gain $\underline{A}$ and $\underline{D}$ can be calculated for each compensation network. To consider the worst case scenario, the tolerance values that minimize $\underline{A}$ and maximize $\underline{D}$ need to be considered in the computation. The results of this example are shown in (5). After this, the actual coefficient a' and d' can be computed to verify which values would these coefficients assume in the worst case scenario of parameters' tolerance.

Fig. 5 shows the resulting a' and d' of the example designs of Section III, when the tolerance of $\pm 5 \%$ is considered for all the circuit parameters. These designs have as initial coefficients a=(1, 1.1, 1.3), and d=(0.7, 0.9, 1). According to Fig. 5(a), the design with a=1.1 does not ensure the validity of the design condition in Table IV for both the S-S and P-S compensations because $a' < 1$ when the worse-case scenario of tolerances is considered. Moreover, when a=1.3, the design condition is still valid as stated by Table IV. On the other hand, according to Fig. 5(b), both designs with d=(0.9, 0.7)
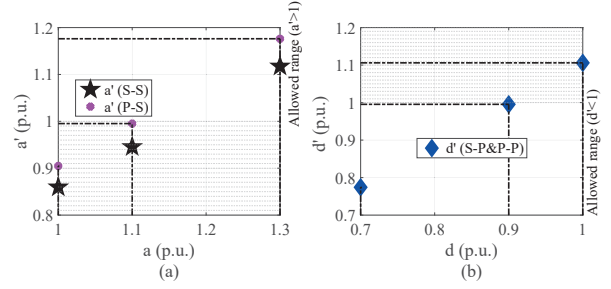
ensure the validity of the design condition in Table IV for both the S-P and P-P compensations because $d' < 1$ when the worse-case scenario of tolerances is considered. However, it needs to be pointed out that the design with d=0.9 just barely satisfies the parametric condition. Even though the parametric condition is satisfied in the presence of parameters' tolerance, it must be ensured that the behavior of the DC/DC converter at the input of the system would still allow the proper controllability of P_{out} when the operating frequency is higher than the resonance to achieve the ZVS turn-on.

$$\underline{A} = \begin{cases} (1-0.05)\sqrt{\dfrac{(1-0.05)^2}{(1+0.05)^2}} = 0.86 & \text{(S-S)} \\[3ex] \sqrt{\dfrac{(1-0.05)^2}{(1+0.05)^2}} = 0.90 & \text{(P-S)} \end{cases}$$

$$\underline{D} = \sqrt{\dfrac{(1+0.05)^2}{(1-0.05)^2}\dfrac{1-0.11^2}{1-(1+0.05)^2 0.11^2}} = 1.11 \quad \text{(S-P \& P-P)}$$
$$\tag{5}$$

As a result, it is essential to consider the parameters' tolerance to ensure the validity of the proposed design condition defined in this paper. The example in Fig. 5 that uses a tolerance of $\pm 5 \%$ for all circuit parameters can be extended to IPT systems with any other tolerance values.

Finally, the entire selection process of the optimized parameters for IPT charging systems based on the coefficient a, or d is summarized Fig. 6.

V. CONCLUSION

In this paper, a guideline on the value of the coils' quality factor has been defined, such that the optimum operation of the coils and the soft-switching of the inverter can be achieved simultaneously for the four basic compensation networks. Examples of this guideline are provided for $11\,\text{kW}$ wireless charging systems. It has been found that the design condition is satisfied when the quality factor of the primary coil is greater than the secondary coil's quality factor. This means that generally, the primary coil's geometry must differ from the one of the secondary coil. Moreover, it has been shown that the choice of the primary coil's quality factor highly influences both the phase angle of the input impedance and the output power characteristic as a function of the frequency. This choice also affects the nominal DC voltage and current at both input
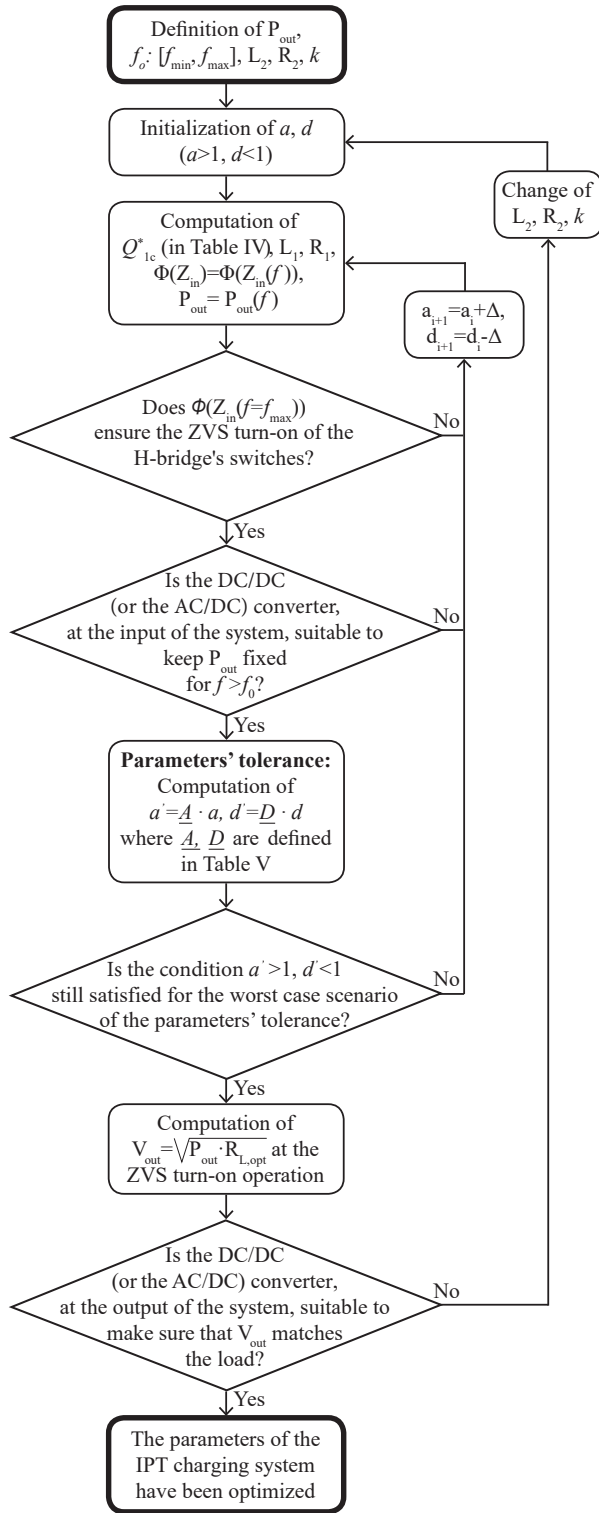
Fig. 6. Flow chart that summarizes the selection process of the optimized parameters for IPT charging systems based on the coefficient a, or d.

and output of the wireless charging systems. In particular, when the quality factor's value of both coils is similar, the phase angles of the input impedance changes smoothly with the frequency, which ensures smooth controllability of the inverter. On the other hand, it must ensure that the DC/DC or

AC/DC converter employed at the input of the system can set a constant output power when the inverter is operating in the inductive region. In fact, depending on the difference between the coils' quality factor, it might be necessary to either step up or step down the DC input voltage. At the same time, the nominal input DC voltage must be within the allowed range from the grid connection, and the nominal output DC voltage must be equal to the battery rated voltage. After this analysis, it has been investigated whether the circuit parameters' tolerance affects the validity of the design condition. It has been found that the design condition's validity could be compromised by considering the standard manufacturing tolerance of $\pm 5\,\%$ for all circuit components. To overcome this, an iterative procedure to adjust the design condition has been explained for the four basic compensation networks such that it takes into account the circuit parameters' tolerance.

REFERENCES

[1] F. Grazian, W. Shi, J. Dong, P. van Duijsen, T. B. Soeiro, and P. Bauer, "Survey on standards and regulations for wireless charging of electric vehicles," in *AEIT International Conference of Electrical and Electronic Technologies for Automotive (AEIT AUTOMOTIVE)*, 2019.

[2] S. Li, W. Li, J. Deng, T. D. Nguyen, and C. C. Mi, "A double-sided lcc compensation network and its tuning method for wireless power transfer," *IEEE Transactions on Vehicular Technology*, vol. 64, pp. 2261 – 2273, 2015.

[3] O. H. Stielau and G. A. Covic, "Design of loosely coupled inductive power transfer systems," in *PowerCon 2000. 2000 International Conference on Power System Technology. Proceedings (Cat. No.00EX409)*, vol. 1, 2000, pp. 85–90 vol.1.

[4] C.-S. Wang, G. Covic, and O. Stielau, "Power transfer capability and bifurcation phenomena of loosely coupled inductive power transfer systems," *IEEE Transactions on Industrial Electronics*, vol. 51, pp. 148 – 157, 2004.

[5] C.-S. Wang, O. H. Stielau, and G. A. Covic, "Design considerations for a contactless electric vehicle battery charger," *IEEE Transactions on Industrial Electronics*, vol. 52, no. 5, pp. 1308–1314, 2005.

[6] S. Chopra and P. Bauer, "Analysis and design considerations for a contactless power transfer system," in *IEEE 33rd International Telecommunications Energy Conference (INTELEC)*, 2011.

[7] M. Iordache, L. Mandache, D. Niculae, and L. Iordache, "On exact circuit analysis of frequency splitting and bifurcation phenomena in wireless power transfer systems," in *2015 International Symposium on Signals, Circuits and Systems (ISSCS)*, 2015, pp. 1–4.

[8] S. Liu, Y. Shen, Y. Wu, J. Lin, and M. Hu, "Study on frequency tracking for wireless power transfer system using magnetic resonant coupling," in *2018 13th IEEE Conference on Industrial Electronics and Applications (ICIEA)*, 2018, pp. 2569–2572.

[9] C.-S. Wang, G. Covic, and O. Stielau, "General stability criterions for zero phase angle controlled loosely coupled inductive power transfer systems," in *27th Annual Conference of the IEEE Industrial Electronics Society (IECON)*, 2001.

[10] W. Zhang and C. C. Mi, "Compensation topologies of high-power wireless power transfer systems," *IEEE Transactions on Vehicular Technology*, vol. 65, no. 6, pp. 4768–4778, 2016.

[11] R. Steigerwald, "A comparison of half-bridge resonant converter topologies," *IEEE Transactions on Power Electronics*, vol. 3, pp. 174 – 182, 1988.

[12] R. Bosshard, J. W. Kolar, and B. Wunsch, "Control method for inductive power transfer with high partial-load efficiency and resonance tracking," in *International Power Electronics Conference (IPEC-Hiroshima - ECCE ASIA)*, 2014.

[13] W. Shi, J. Dong, S. Bandyopadhyay, F. Grazian, T. B. Soeiro, and P. Bauer, "Comparative study of foreign object and misalignment in inductive power transfer systems," in *45th Annual Conference of the IEEE Industrial Electronics Society (IECON)*, 2019.

[14] *J2954 RP: Wireless Power Transfer for Light-Duty Plug-In/ Electric Vehicles and Alignment Methodology*, SAE International Std., Apr. 2019.